Biomedicine & Pharmacotherapy 153 (2022) 113408

Contents lists available at ScienceDirect

Biomedicine & Pharmacotherapy

journal homepage: www.elsevier.com/locate/biopha

Identification of A_{2B}AR as a potential target in colorectal cancer using novel fluorescent GPCR ligands

Jorge Barbazán [a,*], Maria Majellaro [b,*], Antón L. Martínez [c], José M. Brea [c], Eddy Sotelo [d], Miguel Abal [a,e]

[a] Translational Medical Oncology Group (ONCOMET), Health Research Institute of Santiago de Compostela (IDIS), University Hospital of Santiago de Compostela (SERGAS), Trav. Choupana s/n, 15706 Santiago de Compostela, Spain
[b] Celtarys Research S.L., 15706 Santiago de Compostela, Spain
[c] Centro Singular de Investigación en Medicina Molecular y Enfermedades Crónicas (CiMUS), Universidade de Santiago de Compostela, Santiago de Compostela 15782, Spain
[d] Centro Singular de Investigación en Química Biolóxica e Materiais Moleculares (CiQUS) and Departamento de Química Orgánica, Universidade de Santiago de Compostela, Santiago de Compostela 15782, Spain
[e] Centro de Investigacion Biomedica en Red de Cancer (CIBERONC), Monforte de Lemos 3-5, 28029 Madrid, Spain

ARTICLE INFO

Keywords:
Colorectal cancer
GPCRs
Adenosine receptors
Tumor microenvironment
Fluorescent ligands
Drug screening

ABSTRACT

G-protein coupled receptors (GPCRs) have been largely targeted in a wide range of diseases, but few therapies have been directed against GPCRs in the field of cancer, partly because of the lack of effective target identification strategies. Here, using colorectal cancer (CRC) as a model, we explored the gene expression of a panel of GPCRs in tumor and stromal cells, identifying specific gene sets defining each cellular compartment. We selected the adenosine receptor 2B (A_{2B}AR), specifically expressed in cancer cell lines compared with stromal cells, to explore the use of fluorescent ligands that can be used for target visualization. Fluorescent probes allowed semi-quantitative receptor mapping in living cells and validated the specific expression of A_{2B}AR in CRC cell lines. As well, fluorescent ligands were effective at monitoring real-time A_{2B}AR receptor labeling using live-imaging modalities, and displayed high efficiency when used to label complex 3D cellular systems such as tumor spheroids. Finally, we validated A_{2B}AR as a potential pharmacological tool in CRC, using selective antagonists, finding a reduction in tumor cell proliferation. This proof-of-concept study suggests the use of fluorescent ligands for GPCR characterization through imaging, and as possible new tools used for target validation in drug screening methodologies.

1. Introduction

Colorectal cancer (CRC) accounts for approximately 10% of all annually diagnosed cancers and cancer-related deaths worldwide [1]. The majority of CRC (≈90%) are sporadic, while around 5–10% of CRC have a hereditary component [2]. Among new colorectal cancer diagnoses, 20% of patients have metastatic disease at presentation, with a 5-year survival rate of less than 20%, and another 25% presenting with localized disease will eventually develop metastases later on the course of the disease [3]. From a molecular perspective, even if some mutational events are common among CRC (including mutations in *APC*, *TP53*, *KRAS*, *SMAD4* and *PI3CA* [4]), CRC is a highly heterogeneous disease, including hypermutated/ultramutated, microsatellite unstable/stable, immune activated and epigenetically altered tumors [5]. This intrinsic variability highlights the importance of establishing a proper CRC molecular classification, which will impact the clinical stratification of patients, determining the subtype-based targeted interventions that are more suitable for each case. As well, this strengthens the importance of deepen into the molecular characteristics of CRC, which will help in the design of targeted therapies for specific patient subsets.

Recent advances in the structure, interactions, signaling and functions of G protein-coupled receptors (GPCRs), the largest family of cell surface receptors, in the context of cancer have provided new insights into the pathogenesis of CRC and other gastrointestinal tumors [6,7] A well-known example is the chemokine stromal cell-derived factor 1 (SDF1 or CXCL12) and its binding receptor CXCR4. This interaction axis has been attributed key roles across the entire process of tumorigenesis,

* Corresponding authors.

https://doi.org/10.1016/j.biopha.2022.113408
Received 13 April 2022; Received in revised form 29 June 2022; Accepted 11 July 2022
Available online 18 July 2022

including tumor growth, invasion, angiogenesis and metastasis, with a clear prognostic impact for patients with CRC [8]. As well, other GPCRs involved in Adenosine signaling (A_1AR, A_{2A}AR, A_{2B}AR and A_3AR), have been acknowledged as key regulators of the interactions between tumor cells and the tumor microenvironment (TME). High TME concentrations of adenosine, an ATP-derived nucleoside, lead to adenosine-initiated signaling pathways that contribute to tumor growth, for example, through sustained neoangiogenesis, eliciting at the same time the creation of an immunosuppressive environment which hinders immune-based tumor control approaches [9].

However, and even if this evidence clearly indicates the potential of GPCR targeting in cancer, to date only few examples have been successfully used as targets to develop drugs that can block cancer-associated pathways. This is in part due to the lack of molecular probes and screening technologies that allow unequivocal, rapid and cost-effective target identification, visualization and monitoring. Classically, the identification of ligands specifically binding GPCRs has been performed through radioligand binding assays. This technology, developed back in the 1970 s, although highly sensitive for the determination of receptor binding affinities, displays use limitations, such as the restricted availability of radiolabeled ligands, apart from the obvious drawbacks of the use of radioactivity related to safety issues and waste management. As well, GPCR visualization and monitoring has been classically made based on immunocytochemistry or immunohistological assays, employing monoclonal antibodies. However, even if monoclonal antibodies have been developed for this, it is still challenging to obtain specific signals when using antibodies directed to GPCRs. Several other methodologies have been implemented but there's still a need for alternative identification and screening methodologies.

In this work, we carried out a proof-of-concept study in which we screen for GPCRs differentially expressed tumor cells and stromal cells, focusing on cancer associated fibroblasts (CAFs). We validated these results using novel GPCR fluorescent ligands, as effective tools for real-time GPCR visualization in living systems, proving at the same time their potential in image-based drug discovery.

2. Materials and methods

2.1. Cell culture

HCT116, SW480 and SW620 cell lines were purchased from the American Type Culture Collection (ATCC) and cultured in DMEM GlutaMAX (ThermoFisher Scientific), supplemented with 10% Fetal Bovine Serum (FBS) (ThermoFisher Scientific). Cell cultures were regularly tested for the presence of mycoplasma. Human colorectal Cancer Associated Fibroblasts (CAFs) primary cultures were obtained and immortalized as previously reported [10,11], and maintained in DMEM GlutaMAX, 10% FBS, 1% Insulin Transferrin Selenium (ITS) (ThermoFisher Scientific).

To generate HCT116-CAFs cocultures, first HCT116 were seeded and cultured for 2 days in a 33 mm glass-bottom dishes (FluoroDish, World Precision Instruments) to allow them to form well-structured cell islands. Then, CAFs were pre-stained using CellTracker CMFDA green dye (ThermoFisher Scientific), at 10 μM for 30' at 37 °C, washed twice in complete medium, trypsinized and seeded together with cancer cells for 24 h to establish organized cocultures, which were later used for downstream analyses.

2.2. GPCR gene expression analysis

To assess the gene expression of a panel of GPCRs, RNA was first extracted from cell cultures of HCT116, SW480, SW620 and primary CAFs using the RNAeasy Mini kit (Qiagen), following manufacturer's protocol. After RNA quantification (Nanodrop, ThermoFisher Scientific), cDNA was synthesized using the M-muLV reverse transcriptase kit (Roche) as indicated by the manufacturer and used for downstream gene expression analysis. For this, we selected the TaqMan Human GPCR Fast array, which allows for the quantification of 92 of the most relevant human GPCRs, including at the same time 4 different housekeeping genes (*GAPDH*, *18SrRNA*, *GUSB* and *ACTB*). 60 ng of total cDNA were loaded per well, and qPCR was run following standard recommended conditions on a QuantStudio 3 qPCR system (Applied Biosystems).

For data analysis, we selected *GAPDH* and *18SsRNA* as reference genes as they were the ones showing higher expression stability across the analyzed samples. GPCR expression was then calculated as previously reported [12]. Briefly, the relative gene expression for each analyzed GPCR was calculated using the following equation:

$$Relative\quad gene\quad expression = \frac{2^{\Delta Ct\ GoI}}{\mathrm{GeoMean}(2^{\Delta CtREF})}$$

Where, GoI refers to the gene of interest, and REF indicates the reference or housekeeping genes used for the analyses, which were averaged using the geometrical mean (GeoMean). ΔCt values were calculated by subtracting the raw Ct values for each cancer cell line to the Ct value obtained for CAFs, used as normalizer. The final obtained values where then transformed to a Log_2 scale for visualization purposes. Finally, heat maps were built using the open-source software MultiExperiment Viewer (MeV) [13]. Only genes having Ct< 36 values in at least 3 out of the 4 cell lines analyzed were considered for the analysis. The gene expression values scale was limited from − 6.0 to 6.0 (Log_2FoldChange) for amenable visualization purposes. Genes were manually considered CAF or cancer cell specific when following the same trend (towards overexpression or downregulation) in all the analyzed cell lines, so this interpretation should be carefully considered as it might be subjected to user-derived bias.

2.3. Determination of fluorescent ligand's binding affinities

CELT-327 (hA_{2B}/hA_3 fluorescent antagonist) and CELT-228 (hA_3 fluorescent antagonist) were provided by Celtarys Research SL.

Radioligand binding competition assays were performed in vitro using human ARs expressed in transfected HeLa [CHO [hA_1AR (1.5 pmol/mg protein, hA_{2A}AR (9 pmol/mg protein), HEK-293 [hA_{2B}AR (1.5 pmol/mg protein) and hA_3AR (3 pmol/mg protein)] cells as described previously [14–17]. A brief description is given below. A_1AR competition binding experiments were carried out in membranes from CHO-A_1 cells labelled with 1 nM [^{3}H]DPCPX (K_D = 0.7 nM). Non-specific binding was determined in the presence of 10 μM R-PIA. The reaction mixture was incubated at 25 °C for 60 min. A_{2A}AR competition binding experiments were carried out in membranes from HeLa-A_{2A} cells labelled with 3 nM [^{3}H]ZM241385 (K_D = 2 nM). Non-specific binding was determined in the presence of 50 μM NECA. The reaction mixture was incubated at 25 °C for 30 min. A_{2B}AR competition binding experiments were carried out in membranes from HEK-293-A_{2B} cells (Euroscreen, Gosselies, Belgium) labelled with 25 nM [^{3}H]DPCPX (K_D = 21 nM). Non-specific binding was determined in the presence of 400 μM NECA. The reaction mixture was incubated at 25 °C for 30 min. A_3AR competition binding experiments were carried out in membranes from HeLa-A_3 cells labelled with 10 nM [^{3}H]NECA (K_D = 8.7 nM). Non-specific binding was determined in the presence of 100 μM R-PIA. The reaction mixture was incubated at 25 °C for 180 min. After the incubation time, membranes were washed, filtered and radioactivity was detected in a Microbeta Trilux reader (PerkinElmer).

2.4. Confocal imaging

Images were acquired on an inverted confocal microscope (Leica SP8) using laser lanes 405, 488, 561 and 533 nm, an HC-PL-APO CS2 40x/1.30 oil immersion objective, and non-descanned HyD detectors. For each experiment and stage position a Zstack was acquired with a Z-step of 1-2 μm, depending on the experiment. For data visualization, a

representative Z position was selected for each image stack.

All imaging experiments were performed in native non-fixed conditions. To preserve cell viability during imaging, a setup including a CO_2 and temperature incubator was used. Cells were seeded on 33 mm glass-bottom culture dished (Fluorodish, World Precision Instruments) to maximize image acquisition quality. To perform CELT-327 saturation binding assays we used a high content screening system (Operetta, Perkin Elmer). For this, cells were seeded on glass-bottom 96-well plates (CellCarrier 96-Ultra, Perkin Elmer), labelled and imaged using a water immersion 40x objective, and laser lines 405, 488, 561 nm.

HCT116, SW480, SW620 or HCT116/CAF cocultures were cultured until confluence (normally for 48 h) for each experimental setup. Cultures were then counterstained with 10 μM CellTracker CMFDA green dye (ThermoFisher Scientific) and NucBlue™ (at recommended concentrations, ThermoFisher Scientific), otherwise indicated. CELT-327 and CELT-228 and fluorescent XAC (Hellobio) were used at the concentrations indicated for each experimental condition, incubated for 30' at 37 °C in serum free medium, and washed twice with complete medium before imaging. For time-lapse experiments, image stacks were acquired every minute for the indicated channels. After the first 2 acquisitions, CELT-327 250 nM was added to the cell culture medium in serum free medium and imaging continued every minute for 20'. For real-time receptor-dissociation experiments, confluent HCT116 cultures were pre-stained with CELT-327 250 nM and NucBlue, imaged for 5 acquisitions (1 per minute), and then MRS1220 was added to a final concentration of 10 μM. Ligand dissociation was then monitored for the indicated time, acquiring 1 frame per minute.

2.5. MRS1220 competition assays

Ligand competition assays were performed in the same culture conditions as previously reported. HCT116 cells were seeded on 33 mm glass-bottom dishes or in glass-bottom 96-well plates (CellCarrier 96-Ultra, Perkin Elmer), for 48 h until confluence. For sequential competition assays, cells were first incubated with CELT-327 at 250 nM for 30' at 37 °C in serum free medium, washed twice with complete medium and imaged. Then, without further washing steps, cells were incubated in a solution of 10 μM MRS1220 (Sigma Aldrich M228) in serum-free medium for another 30' at 37 °C and directly imaged. At this saturating concentration, MRS1220 works as a non-selective $A_{2B}AR/A_3AR$ antagonist, displacing CELT-327 binding in HCT116 cells (Ki (A_{2b})= 332 nM [18], Ki(A_3)= 0.65 nM [19]. For simultaneous competition assays, both CELT-327 (at indicated concentrations) and MRS1220 (10 μM) were added simultaneously to cell cultures in serum free medium, incubated for 30' at 37 °C and imaged directly without further washing.

2.6. Proliferation assays

ISAM140, $A_{2B}AR$ selective antagonist and ISVY-74, A_3AR selective antagonist, were synthesized according to the procedures previously published by our group [8,9]. The effect ISAM140 and ISVY-74 on the proliferation of HCT116 cells was tested by plating 2000 cells/well on a 96-well plate overnight in complete medium. Cells were then incubated for another 24 h with solutions containing either ISAM140 or ISVY-74 at 2 μM in complete medium. Controls with the equivalent amount of DMSO, used as the solvent for the indicated antagonists, were as well performed. After incubation, the number of viable cells was determined by using AlamarBlue (ThermoFisher Scientific) following manufacturer's recommendations. Proliferation rates for each condition were represented as % proliferation respect to the appropriate DMSO controls.

2.7. Image analysis and statistics

Images were analyzed using ImageJ (Fiji) v.2.3.0/1.53f. Average fluorescence signals for given channels, planes and time points were measured and plotted as arbitrary units. For spheroid experiments, a plane located at 60 μm deep from the first Z-section with detectable signal was chosen for the analysis. The distribution of fluorescence signals for all analyzed channels in XY-plane was quantified by averaging the fluorescence intensity of all pixels located in a 180 px width line positioned across the spheroid equatorial plane. Intensity signals along line length for each spheroid was discretized in %, to generate data comparable across all the spheroids analyzed, due to differences in spheroid size. 100 μm orthogonal projections were generated in the Z dimension, and average fluorescence intensity signals were measured over a 100 μm/300 px line section and plotted as % respect to the maximum intensity signal for each channel.

3D visualization of spheroid staining was perform using Imaris 7.2.3 (Bitplane). Data was analyzed and plotted using GraphPad Prism 9. Statistical test and significance values are indicated for each independent experiment on the corresponding figure legend.

3. Results

3.1. Identification and validation of a specific tumor-related GPCR-based gene expression signature

To identify CRC-specific GPCRs, the expression of 92 GPCRs (Supplementary Table 1) was analyzed by RTqPCR in three colorectal cancer cell lines, HCT116, SW480 and its lymph node metastatic derivative cell line, SW620. Although limited in number, this gene panel covers some of the most relevant GPCR functions described in cancer. We compared this with their expression in primary CAFs, the main non-tumoral component of the TME in CRC, used as a normalizer to get the relative expression levels in tumor cells (Fig. 1A). 38 out of 92 (41%) of the analyzed genes showed detectable expression levels, (Cq <36 in at least 3 out of 4 samples). 7 GPCR genes were found mainly or exclusively expressed in CAFs (Fig. 1A, orange label), while the expression of 10 of the analyzed GPCRs was restricted to tumor cells (Fig. 1A, magenta label). The rest of the genes didn't show a robust expression pattern in all CRC cell lines to be classified as cancer-specific, although many of them were found highly overexpressed in at least 2 CRC cell lines, compared to CAFs expression. As expected, the expression of the Alpha-Chemokine Receptor CXCR4 specific for the Stromal-Derived-Factor-1 (SDF-1), involved in chemotaxis and metastatic dissemination in CRC, among other cancers, was homogenously increased in all CRC cell lines. Interestingly, we found correlative expression of certain gene families, such as for the Cadherin EGF LAG Seven-Pass G-Type Receptors 1, 2 and 3 (*CELSR1*, *CELSR2* and *CELSR3*), all found to be highly and specifically expressed in the CRC cell lines, or the Atypical Chemokine Receptors 3 and 4 (*ACKR3* and *ACKR4*), exclusively expressed in CAFs. Adenosine receptors exhibited a variable expression pattern, with *ADORA3* showing undetectable expression levels, *ADORA1* preferentially expressed in CAFs, while *ADORA2A* and *ADORA2B* displayed an unequivocal tumor-specific expression pattern (Fig. 1A,B).

This initial profiling allowed us to identify both tumor and stromal-specific GPCRs, as candidates for the exploration of fluorescence-based imaging probes, useful for live target visualization, quantification, and as tools for possible drug screening methodologies. For this, we selected the family of adenosine receptors in a proof-of-concept validation and employed a fluorescently-labeled ligand (CELT-327) based on a proprietary synthetic strategy (Celtarys Research). This fluorescent ligand binds selectively $A_{2B}AR$ and A_3AR subtypes with high affinity (Ki= 35.6 nM for $A_{2B}AR$ and 45.7 nM for A_3AR), emitting in the red region of the visible spectrum as it is linked to a Bodipy-Texas Red fluorophore ($\lambda exc.$ 589 nm – $\lambda em.$ 616 nm).

CELT-327 was then used to determine both the relative expression and localization of $A_{2B}AR$ and A_3AR, which can be performed in real time in living cellular systems, due to the compatibility of this type of ligands with cell culture methodologies, and detectable using standard

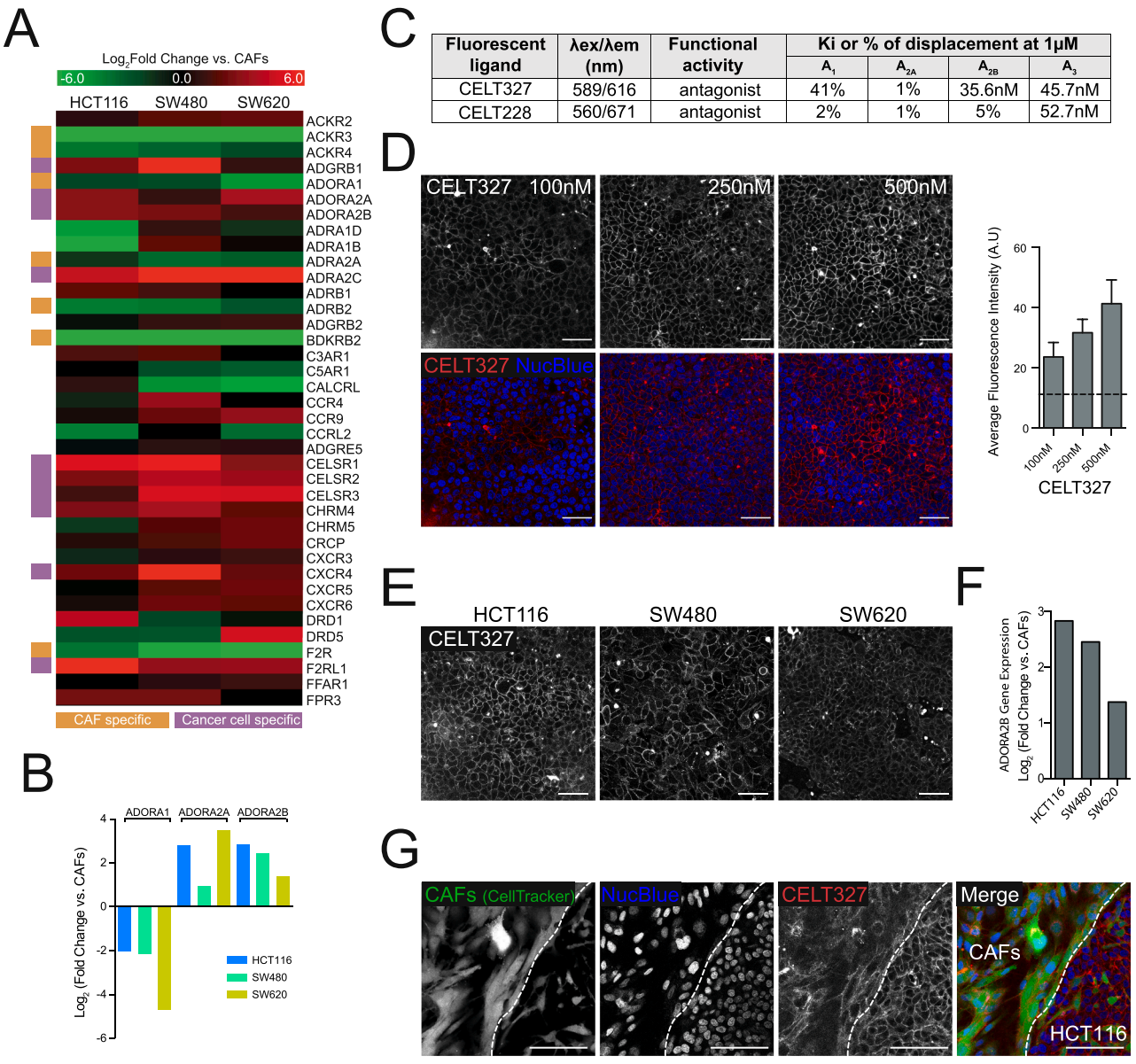

Fluorescent ligand	λex/λem (nm)	Functional activity	Ki or % of displacement at 1μM			
			A_1	A_{2A}	A_{2B}	A_3
CELT327	589/616	antagonist	41%	1%	35.6nM	45.7nM
CELT228	560/671	antagonist	2%	1%	5%	52.7nM

Fig. 1. A_{2B}AR is specifically expressed in colorectal cancer cell lines. A) Heatmap showing gene expression values of a panel of detectable GPCRs in 3 colorectal cancer cell lines, versus their expression in primary human cancer associated fibroblasts (CAFs). Gene expression values are represented in Log_2FoldChange and colour maps are saturated beyond (-6,6) expression range. GPCRs of particular interest are labelled based on their specific expression in cancer cells (magenta) or CAFs (orange). B) Gene expression values of the adenosine receptors gene family in cancer cell lines versus CAFs. *ADORA3* is not represented in the graph as is displayed no detectable gene expression signal in the cell lines tested. C) Fluorescent ligands general properties. % of displacement and Ki values are determined by radioligand binding assays as detailed in the material and method section. D) Representative confocal images of HCT116 cells labelled with increasing concentrations of CELT-327. Dashed line represents the average background fluorescence noise. Average fluorescence intensity quantifications shown in right panel (n = 3), Scale bars: 50 μm E) Representative confocal images of HCT116, SW480 and SW620 cells stained with 250 nM CELT-327. Scale bars: 50 μm F) Gene expression values of the A_{2B}AR measured by qPCR in HCT116, SW480 and SW620 cell lines, n = 1. G) Representative confocal images of cocultures of HCT116 cells and human primary CAFs. Dashed line represents the frontier between both cell types. CAFs are labelledwith CellTracker (Green), and cocultures labelled with CELT-327 250 nM. Scale bar 100 μm.

confocal-based imaging modalities. As shown in Fig. 1D and Supplementary Figure 1, CELT-327 showed a specific and dose-dependent membrane fluorescent labeling in HCT116 cells, at concentrations at the nanomolar range, saturating between 500 and 750 nM. We selected 250 nM as the optimal concentration for further experiments, as it provides well-detectable fluorescence above noise levels, avoiding possible out-of-range saturation artifacts occurring at higher ligand concentrations. A similar membrane-specific staining was observed in SW480 and SW620 cell lines (Fig. 1E), with labeling levels correlating with the expression of the *ADORA2B* gene, measured by qPCR (Fig. 1F), thus validating the relative quantitative features of this type of ligands. Of note, the expression of the *ADORA3* gene is absent in all tested cell lines, indicating that the signal detected using CELT-327 comes exclusively from the expression of A_{2B}AR. This was confirmed in parallel using a second labeled ligand, CELT-228, which selectively binds the A_3AR (Fig. 1B), and displays no signal in HCT116, SW480 or SW620 cells, while showing a strong and specific signal in HeLa cells stably expressing A_3AR (HeLa-A_3) (Supplementary Figure 2). Interestingly, using live cocultures of HCT116 and human primary CAFs, we detected an increased tumor-specific labeling of CELT-327 (Fig. 1G), in agreement with the relative expression values reported above, further confirming A_{2B}AR as a specific tumor GPCR in CRC, and CELT-327 as a

robust detection probe.

3.2. Real-time imaging of A_{2B}AR labeling dynamics

To understand the binding dynamics of CELT-327, we carried out a confocal-based live imaging labeling experiment, which allowed us to visualize receptor binding in real time. As shown in Fig. 2 and Supplementary movie 1, a detectable fluorescence signal started to appear only one minute after the addition of CELT-327, becoming evident and membrane-specific at minute 2, and increasing exponentially until a saturation plateau after approximately 10 min (Fig. 2A-C). We detected a fluorescence intensity decrease after 20 min of imaging, mainly attributed to photobleaching (Fig. 2C). Considering that the fluorescent ligand needs to diffuse within the culture medium before reaching the cells, these results indicate a fast and stable staining of the A_{2B}AR using CELT-327. As well, we validated the rapid diffusion and homogeneous distribution of CELT-327 within the cell monolayer, staining both apico-basal and lateral membranes, as observed after projecting the obtained images in the orthogonal dimension (Fig. 2B).

Supplementary material related to this article can be found online at doi:10.1016/j.biopha.2022.113408.

3.3. Efficient labeling of A_{2B}AR in cellular systems of increased complexity

To validate the use of this type of fluorescently-labeled ligands, we compared the labeling efficiency of CELT-327 with other commercially available fluorescent probes targeting the A_{2B}AR (fluorescent XAC). Using the same labeling conditions and ligand concentrations, while both ligands specifically labeled membrane structures within the cell cultures, it was observed an improved membrane labeling in terms of the average intensity when using CELT-327 (Fig. 3A). However, even if we detected obvious differences between both dyes, it is important to highlight that the two ligands contain different fluorophores. Therefore, even if they are excited at equivalent laser powers at the corresponding excitation wavelength, there could be a limitation in the resulting labeling comparison.

The field of marker identification in cancer biology is trending towards the analysis of complex tissue-like cellular structures, for example 3D spheroids or organoids, which recapitulate more faithfully the *in vivo* tumor scenario, allowing obtaining data using *in vitro* models without the need of animal experimentation. However, one of the main constraints when performing live imaging of such complex structures resides on the limited penetration of fluorescent antibodies and available dyes, loosing relevant information from areas located at deep regions. Accordingly, we sought to evaluate the performance of CELT-327 in staining 3D live complex structures like HCT116 compact spheroids. For these experiments (Fig. 3B-D) we comparatively analyzed the staining with two well-known small-molecule dyes: CellTracker and NucBlue. CellTracker, which stains the cytoplasm of live cells, and NucBlue, a derivative of Hoechst 33342 that stains DNA, were only effective at labeling cells at the surface of the spheroid. In clear contrast, CELT-327 displayed a homogeneous staining across the entire spheroid diameter (Fig. 3B top panel, and C), reaching deep spheroid regions (Fig. 3B lower panel, and D) (Supplementary Movie 2). Altogether, these results indicate that probes such as CELT-327 display improved diffusion and penetration abilities, maximizing the power of live imaging in complex tissues.

Supplementary material related to this article can be found online at doi:10.1016/j.biopha.2022.113408.

3.4. A_{2B}AR targeting as a potential pharmacological tool in CRC

Upon this comprehensive characterization of the specificity and performance of the CELT-327 fluorescent ligand in different in vitro models, we aimed at demonstrating its applicability as a versatile and easy-to-use preclinical tool for the pharmacological targeting of the A_{2B}AR in the context of CRC. For this, we performed a proof-of-concept study with known A_{2B}AR antagonists combining competitive binding/displacement and cell viability. Specific binding was confirmed in competition assays where HCT116 cells were incubated with increased concentrations of CELT-327 together with unlabeled MRS1220, which acts as non-selective A_{2B}AR/A_3AR antagonist when used at saturating concentrations (10 μM). MRS1220 completely displaced CELT-237 binding at 250 nM, and in a high extent at increased concentrations of CELT-327 (Fig. 4A, middle panels, and Supplementary Figure 1). Similar results were obtained when CELT-327 (250 nM) and MRS1220 (10 μM) were added to the cell cultures sequentially, (Fig. 4A, right panels). This was as well monitored in real-time, by performing time-lapse imaging of HCT116 cells pre-labeled with 250 nM CELT-327. Upon addition of 10 μM MRS1220, we observed a rapid decrease in the fluorescence signal over time (≈90% in 10 mins), which was specific from ligand dissociation, and not due to fluorophore bleaching (Fig. 4 B,C, Supplementary Movie 3). These results validated CELT-327 as a tool for the further development of imaging-based methodologies aimed at screening for specific compounds selectively targeting A_{2B}AR. Finally, and in order to prove the functional relevance of A_{2B}AR targeting, we analyzed the effectiveness of selective A_{2B}AR antagonists in blocking

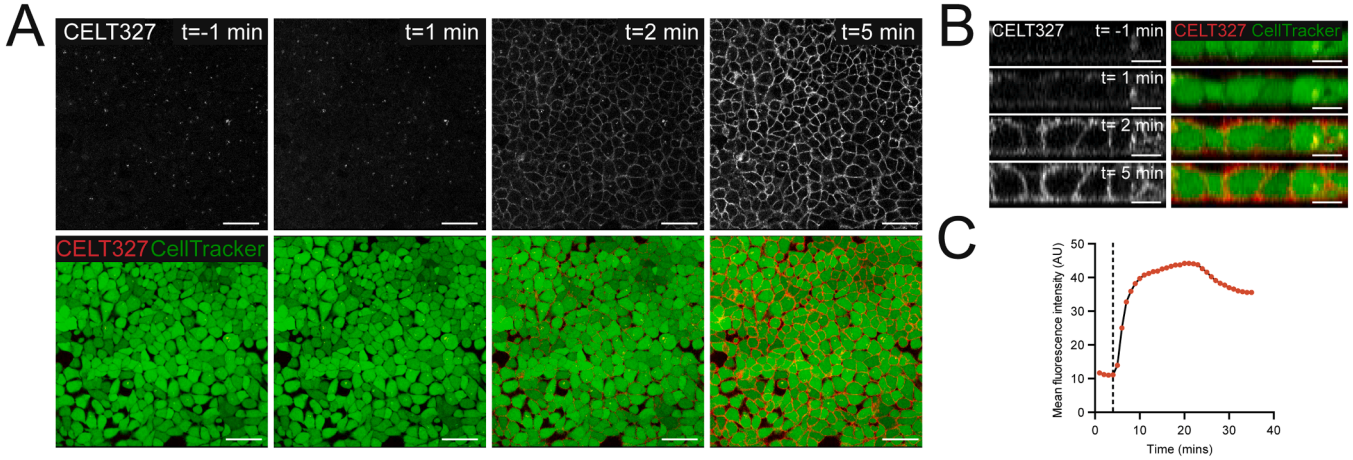

Fig. 2. Real-time dynamic labelling of A_{2B}AR. A) Representative confocal images of HCT116 cells pre-stained with CellTracker Green (lower panels), and labelled in real-time with CELT-327 250 nM, added at timepoint 0 (upper panels). Scale bars: 50 μm. B) Orthogonal projections on a selected area of images in A. Scale bar: 20 μm. C) Quantification of CELT-327 average fluorescence intensity over time.

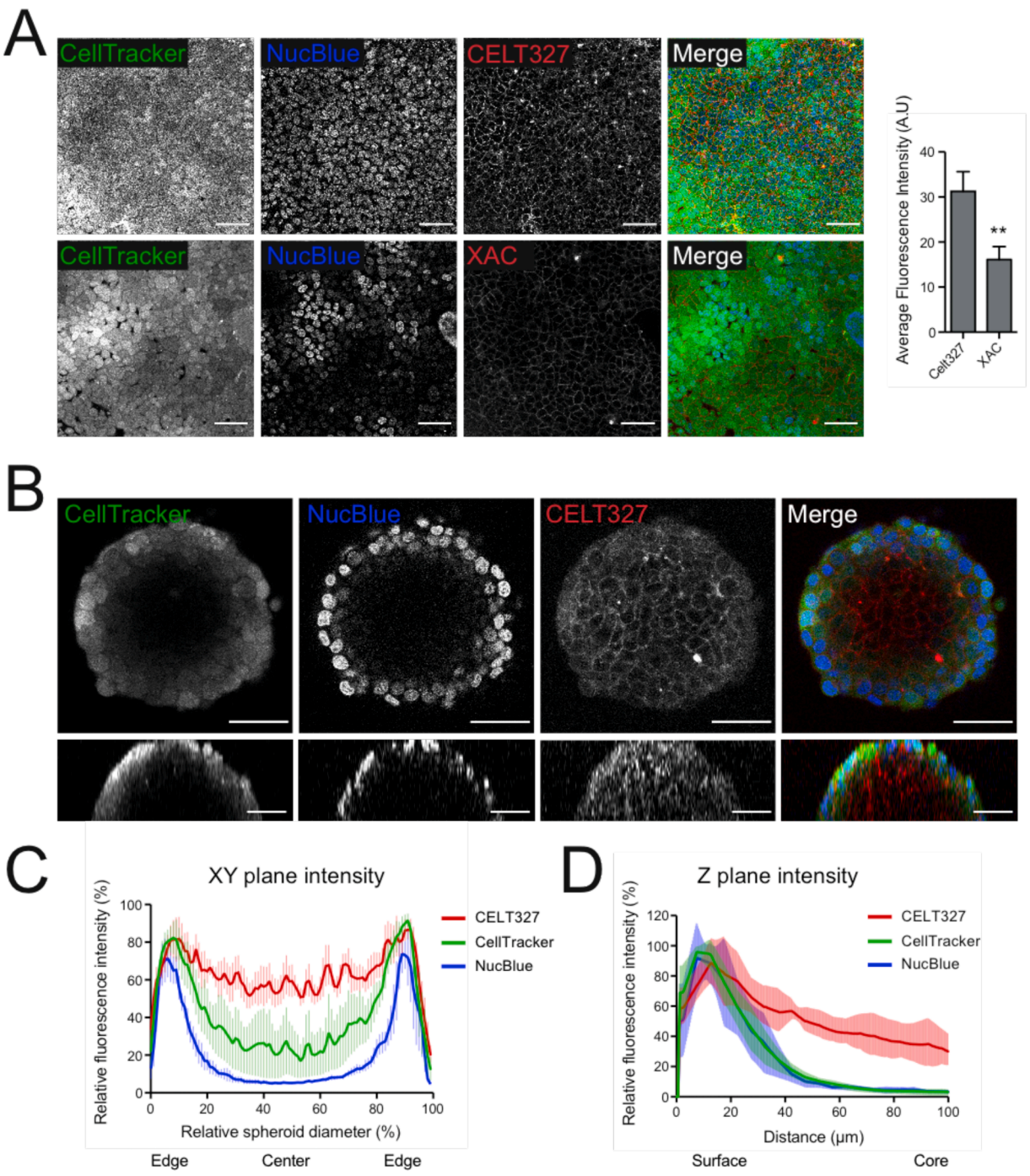

Fig. 3. CELT-327 labelling efficiency in 2D and 3D cell cultures. A) Representative images of non-fixed HCT116 labelled with CELT-327 (upper panels) and fluorescent XAC (lower panels) at 250 nM. Scale bars: 50 μm. Right plot: average fluorescence intensity quantification. **p < 0,01, Mann-Whitney test. B) HCT116 3D spheroids co-stained simultaneously with CELT-327 250 nM, CellTracker Green (10 μM) and NucBlue. Upper panels: XY projections. Lower panels: Z projections. Scale Bars: 50 μm. C) Average fluorescence intensity quantification of labelled spheroids on a 60 μm-deep XY plane (n = 4). Spheroid diameter was normalized to a % scale for plotting purposes. D) Average fluorescence intensity quantification of labelled spheroids orthogonal Z projections (n = 4).

cell proliferation. HCT116 cells were incubated in the presence of ISAM140, a high affinity A_{2B}AR antagonist (Ki = 3.49 nM) [14], or ISVY-74, a pyrimidine derivative eliciting high affinity (Ki = 3.6 nM) and selectivity towards the A_3AR [20]. After 24 h of incubation at physiological concentrations, we observed a slight but consistent and significant reduction in proliferation only in the presence of the A_{2B}AR antagonist, while no effect was found in the presence of the selective A_3AR ligand (Fig. 4D), concordant with the gene expression pattern of such receptors in this cell line (Fig. 1).

Supplementary material related to this article can be found online at doi:10.1016/j.biopha.2022.113408.

These results validated the usefulness of fluorescent GPCR ligands, and in particular for the A_{2B}AR, as a preclinical tool for the comprehensive characterization of GPCRs using live imaging modalities and offering the starting point for the design of new spatially-resolved expression studies, drug screening platforms, or ligand-binding interactions analyses in cancer.

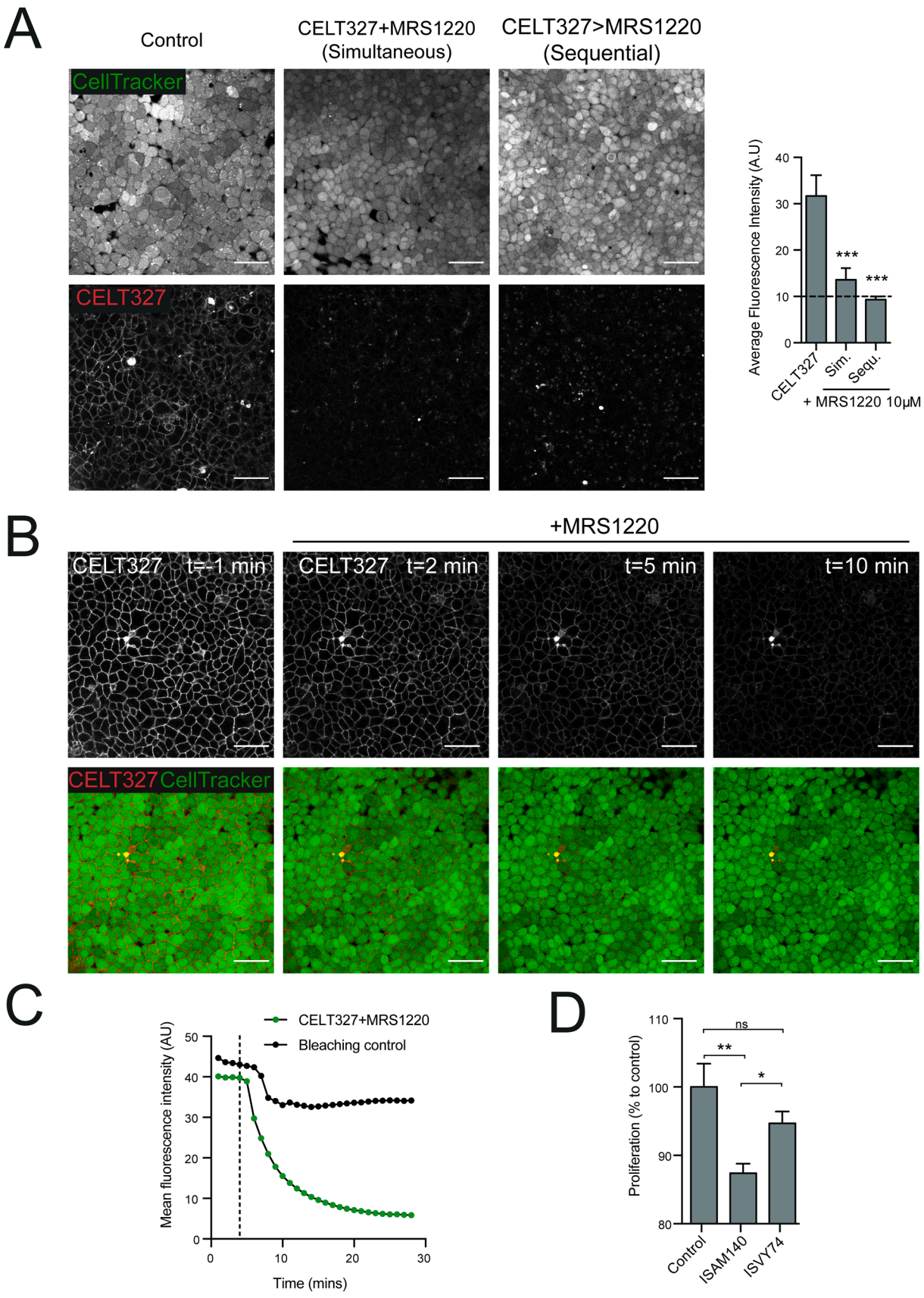

(caption on next page)

Fig. 4. Proof-of-concept study of A_{2B}AR targeting in CRC. A) Representative images of competition binding assays using CELT-327 and MRS1220 as a non-labelled ligand in HCT116 live cells. Left panels: CELT-327 250 nM control. Middle panels: Receptor labelling upon simultaneous incubation of cells with CELT-327 250 nM and MRS1220 10 μM (concentration at which MRS1220 is an A_{2B}AR/A_3AR antagonist). Right panels: Receptor labelling upon sequential incubation of cells, first with CELT-327 250 nM and then with MRS1220 10 μM. Right plot: Quantification of average fluorescence intensity. Dashed line indicates fluorescence noise levels (n = 2, *** p < 0001, Mann-Whitney test). B) Representative confocal images of HCT116 cells pre-stained with 250 nM CELT-327 and CellTracker Green, to which 10 μM MRS1220 is added at timepoint 0, and fluorescent ligand displacement monitored in real-time. Scale bars: 50 μm. C) Quantification of CELT-327 average fluorescence intensity over time in the presence of MRS1220 (green dots). Vertical dashed line indicates the timepoint of MRS1220 addition. Black dots represent a bleaching control where no compound is added. D) Quantification of HCT116 proliferation when incubated for 24 h either with DMSO as a control or with ISAM140 (A_{2B}AR antagonist) or ISVY-74 (A_3AR antagonist) (n = 2, ** p < 0,01; * p < 0,05; ns: non-significant, ANOVA, Friedman test).

4. Discussion

Although GPCRs have been attributed several key roles in the initiation and development of different cancer types, including colorectal, only recently a few of them have been targeted in order to inhibit relevant cancer-associated pathways. One example is the A_{2B}AR, which has been increasingly related to tumor progression, as a regulator of tumor cell features such as proliferation, angiogenesis, metastasis, chemoresistance and immune evasion [21]. This, together with its elevated expression in cancer versus normal adjacent tissues [21], makes it a promising target against CRC, but still, the chemical space explored by the current A_{2B}AR ligands is limited, where the best characterized A_{2B}AR antagonists are mainly xanthine congeners [22].

While few compounds have reached clinical trials [23], much remains to be explored in the field of GPCR-based target development in cancer. One of the main setbacks hindering the definitive entry of GPCR-based cancer therapies in the clinics relies on the identification of potent and selective targets and, with some of the classical discovery methodologies becoming obsolete, there's a clear need of new tools that allow pushing the field forward. In this work, we document the use of fluorescent probes to study the expression, visualization and validating A_{2B}AR as an attractive therapeutic target in CRC, but also preliminarily demonstrating the potential of these tools in the identification of new selective compounds.

To design probes suitable for CRC profiling, we performed an unbiased gene expression pilot study using colorectal cancer cell lines as a model. Comparing their expression levels with the ones detected in CAFs, which represent the vast majority of cells within the TME in colorectal cancers, allowed us to identify GPCRs specific for both tumor and non-tumor cell populations. We selected the A_{2B}AR for the development of fluorescent ligands (CELT-327), due to the importance that adenosine plays in cancer development, especially because of its relationship with the effectiveness of immunotherapies. Importantly, these results validate previous results from our group showing the involvement of the A_{2B}AR in prostate cancer progression [24], extending them to colorectal cancer, and confirming the tumor cell selectivity of the A_{2B}AR compared with other cells from the TME. Still, as this is a reductionist model of the tumor complexity, the expression pattern of the A_{2B}AR should be expanded to other cell types of the microenvironment. As well, even if this work focuses particularly on the A_{2B}AR, ligands against other protein families found as tumor or CAF-specific are already under development.

The CELT-327 probe (and also CELT-228, which was not further characterized in this work), labels cell membranes on a fast, stable and specific manner, showing optimal performance in live imaging modalities, and outperforming currently available tools. This allowed us to monitor receptor labeling in real time and in native, non-fixed cells, which ensures maximal preservation of native receptor structures, and positions these fluorescent ligands as useful tools for live receptor trafficking studies. Moreover, these types of probes are efficient at labeling A_2ARs in complex tissue-like cellular structures like spheroids, offering efficient future tools for GPCR imaging in advanced microscopy systems such as 2-photon *ex vivo* tissue imaging or intravital microscopy. As well, the selectivity, binding and specificity properties of these probes make them optimal for the development of cell-based assays to screen compounds targeting given GPCRs.

A_{2B}AR antagonism is being explored both at the preclinical [25] and clinical [23] levels, and its involvement in several processes of the tumorigenic cascade will demand the development of alternative targeting strategies in the near future. Although preliminary, the proof-of-concept study we performed with ISAM140 (A_{2B}AR selective antagonist) on tumor cell proliferation, guarantees further screenings in large compound libraries aimed at identifying new potent GPCR agonists/antagonists, or for GPCR deorphanization.

5. Conclusions

In short, we used a fluorescent ligand and live imaging microscopy methodologies as an attractive strategy to comprehensively characterize A_{2B}AR in the context of CRC. The reported findings constitute a proof of concept for the optimization of new screening assays to identify and validate novel targeted therapies against CRC.

Conflicts of interest

María Majellaro is Chief Scientific Officer of Celtarys Research SL.

Acknowledgements

We gratefully thank Sonia Martinez-Arca and Maria I. Loza for fruitful experiment discussions and critical reading of the manuscript.

This work was supported by the Juan de la Cierva grant program to Jorge Barbazán (IJC2018-036875-I) and CIBERONC (CB16/12/00328). We also thank the Consellería de Cultura, Educación e Ordenación Universitaria of the Galician Government (grant: ED431B 2020/43), Centro Singular de Investigación de Galicia accreditation 2019–2022 (ED431G 2019/03) and the European Regional Development Fund (ERDF), Ministerio de Ciencia e Innovación-Agencia Estatal de Investiogación-FEDER-EU (PID2021-124010OB-100) for the financial support.

Appendix A. Supporting information

Supplementary data associated with this article can be found in the online version at doi:10.1016/j.biopha.2022.113408.

References

[1] J. Ferlay, et al., Cancer incidence and mortality patterns in Europe: estimates for 40 countries in 2012, Eur. J. Cancer 51 (2013) 1201–1202.
[2] T. Sawicki, et al., A review of colorectal cancer in terms of epidemiology, risk factors, development, symptoms and diagnosis, Cancers 13 (2021) 1–23.
[3] L.H. Biller, D. Schrag, Diagnosis and treatment of metastatic colorectal cancer: a review, JAMA 325 (2021) 669–685.
[4] D.M. Muzny, et al., Comprehensive molecular characterization of human colon and rectal cancer, Nature 487 (2012) 330–337.
[5] C. Soneson, et al., The consensus molecular subtypes of colorectal cancer, Nat. Med. 21 (2016) 1350–1356.
[6] R. Bar-Shavit, et al., G protein-coupled receptors in cancer, Int. J. Mol. Sci. 17 (2016) 1–16.
[7] Z. Zeng, et al., Roles of g protein-coupled receptors (Gpcrs) in gastrointestinal cancers: Focus on sphingosine 1-shosphate receptors, angiotensin ii receptors, and estrogen-related gpcrs, Cells 10 (2021) 1–27.
[8] T. Khare, M. Bissonnette, S. Khare, Cxcl12-cxcr4/cxcr7 axis in colorectal cancer: Therapeutic target in preclinical and clinical studies, Int. J. Mol. Sci. 22 (2021).

[9] V. D'antongiovanni, et al., The adenosine system at the crossroads of intestinal inflammation and neoplasia, Int. J. Mol. Sci. 21 (2020) 1–17.
[10] Barbazan, J. et al., 2021. Cancer-associated fibroblasts actively compress cancer cells and modulate mechanotransduction. *bioRxiv* 2021.04.05.438443 (2021).
[11] A. Glentis, et al., Cancer-associated fibroblasts induce metalloprotease-independent cancer cell invasion of the basement membrane, Nat. Commun. 8 (2017) 1–13.
[12] J. Hellemans, G. Mortier, A. De Paepe, F. Speleman, J. Vandesompele, qBase relative quantification framework and software for management and automated analysis of real-time quantitative PCR data, Genome Biol. 8 (2008).
[13] A.I. Saeed, et al., TM4: A free, open-source system for microarray data management and analysis, Biotechniques 34 (2003) 374–378.
[14] A. El Maatougui, et al., Discovery of potent and highly selective A2B adenosine receptor antagonist chemotypes, J. Med. Chem. 59 (2016) 1967–1983.
[15] C. Carbajales, et al., Enantiospecific recognition at the A2B adenosine receptor by alkyl 2-Cyanoimino-4-substituted-6-methyl-1,2,3,4-tetrahydropyrimidine-5-carboxylates, J. Med. Chem. 60 (2017) 3372–3382.
[16] A. Mallo-Abreu, et al., Trifluorinated pyrimidine-based A2B antagonists: optimization and evidence of stereospecific recognition, J. Med. Chem. 62 (2019) 9315–9330.
[17] A. Crespo, et al., Discovery of 3,4-Dihydropyrimidin-2(1H)-ones as a novel class of potent and selective A2B adenosine receptor antagonists, ACS Med. Chem. Lett. 4 (2013) 1031–1036.
[18] M. Stewart, et al., [3H]OSIP339391, a selective, novel, and high affinity antagonist radioligand for adenosine A2B receptors, Biochem. Pharmacol. 68 (2004) 305–312.
[19] Y.C. Kim, X.D. Ji, K.A. Jacobson, Derivatives of the triazoloquinazoline adenosine antagonist (CGS15943) are selective for the human A3 receptor subtype, J. Med. Chem. 39 (1996) 4142–4148.
[20] V. Yaziji, et al., Pyrimidine derivatives as potent and selective A3 adenosine receptor antagonists, J. Med. Chem. 54 (2011) 457–471.
[21] Z.G. Gao, K.A. Jacobson, A2b adenosine receptor and cancer, Int. J. Mol. Sci. 20 (2019) 1–18.
[22] K.A. Jacobson, D.K. Tosh, S. Jain, Z.G. Gao, Historical and current adenosine receptor agonists in preclinical and clinical development, Front. Cell. Neurosci. 13 (2019) 1–17.
[23] J.D. Powderly, et al., AB928, a novel dual adenosine receptor antagonist, combined with chemotherapy or AB122 (anti-PD-1) in patients (pts) with advanced tumors: Preliminary results from ongoing phase I studies, J. Clin. Oncol. 37 (2019) 2604.
[24] M. Majellaro, et al., 3,4-Dihydropyrimidin-2(1H)-ones as antagonists of the human A2BAdenosine receptor: optimization, structure-activity relationship studies, and enantiospecific recognition, J. Med. Chem. 64 (2021) 458–480.
[25] D.F. Ma, et al., Hypoxia-inducible adenosine A2B receptor modulates proliferation of colon carcinoma cells, Hum. Pathol. 41 (2010) 1550–1557.